Weak gravitational lensing and the Euclid space mission

Martin Kilbinger

CEA Saclay, Irfu/DAp - AIM, CosmoStat; IAP

École polytechnique, enseignement d'approfondissement
13 novembre 2018

martin.kilbinger@cea.fr
www.cosmostat.org/kilbinger
Slides: http://www.cosmostat.org/people/kilbinger
@energie_sombre

Overview

Basics of cosmology

Basics of gravitational lensing

Weak lensing measurement

Results from current surveys

Euclid

Books, Reviews and Lecture Notes

- Kochanek, Schneider & Wambsganss 2004, book (Saas Fee) Gravitational lensing: Strong, weak & micro. Download Part I (Introduction) and Part III (Weak lensing) from my homepage `http://www.cosmostat.org/people/kilbinger`.
- Kilbinger 2015, review Cosmology from cosmic shear observations Reports on Progress in Physics, 78, 086901, arXiv:1411.0155
- Mandelbaum 2018, review Weak lensing for precision cosmology, ARAA submitted, arXiv:1710.03235
- Sarah Bridle 2014, lecture videos (Saas Fee) `http://archiveweb.epfl.ch/saasfee2014.epfl.ch/page-110036-en.html`

Cosmology: The science of the Universe

Matter-energy content

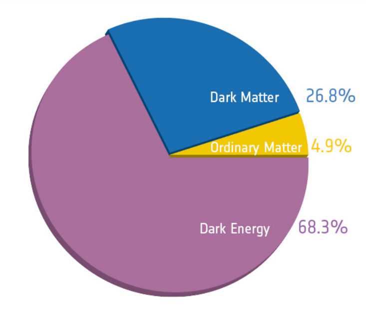

(+ photons, neutrinos)
[Planck Collaboration, 2018]

Expansion history

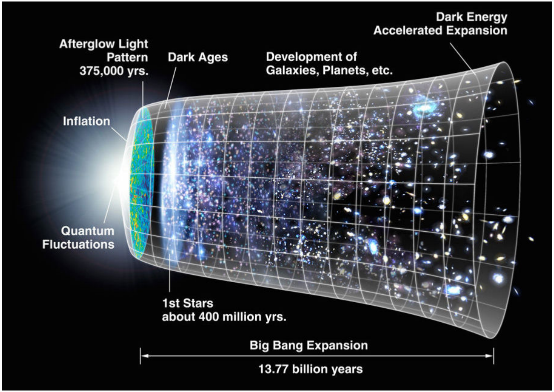

"Standard model": Flat ΛCDM cosmology.

Cosmology: The science of the Universe

Structure formation

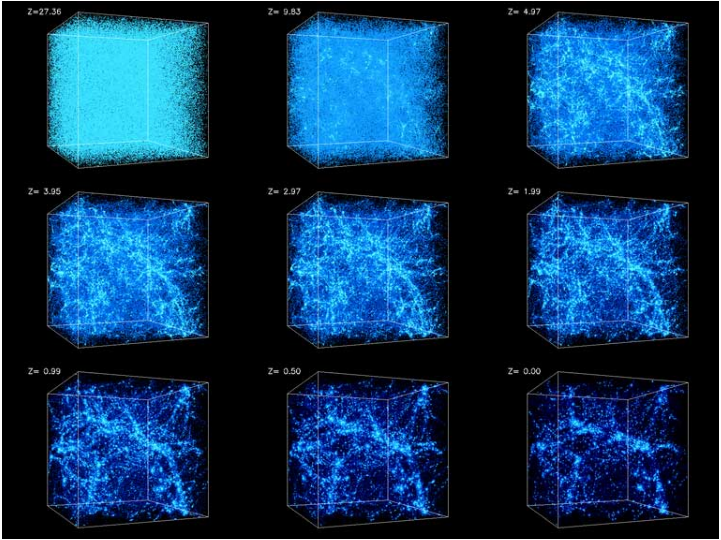

Galaxies and dark matter; (Springel et al. 2005), 10^{10} simulated particles

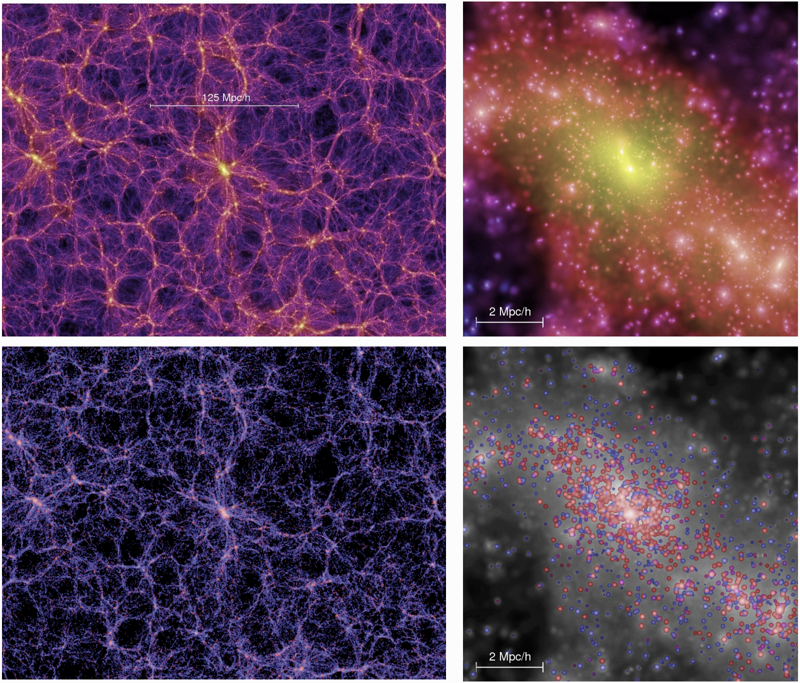

Dark matter

Indirect detection

Example: galaxy rotation curves.

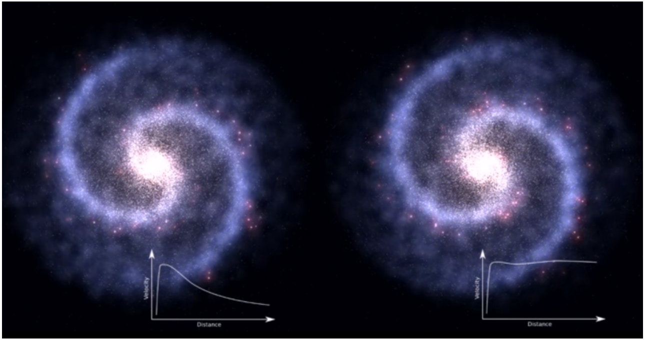

Also gravitational lensing.

Direct detection

Large under-ground experiments, no detection so far.

Dark energy

Indirect detection: Supernovae type Ia = “standard candles”

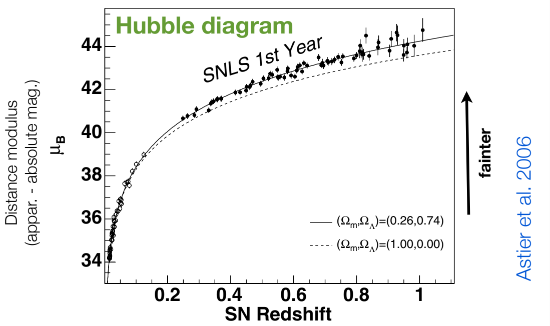

SNIa = “standard candles”, absolute luminosity (more or less) fixed, relative luminosity (magnitude) only depends on distance.

Dark energy

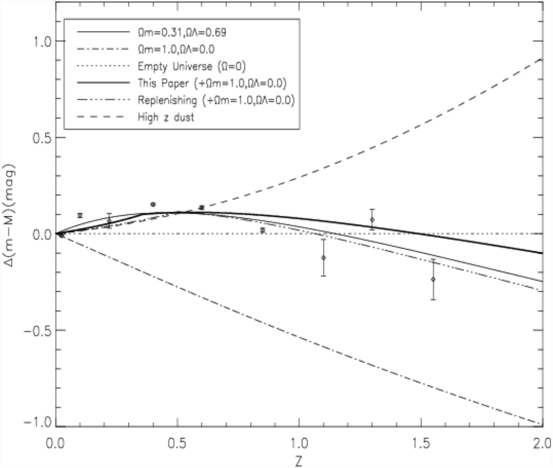

SNIa fainter than for matter-only universe at medium redshift z;
But seems to follow matter-dominated law at high z, too bright for dust absorption of light.

Nature of dark energy?

Einstein equations:

$$R_{\mu\nu} - \frac{1}{2} g_{\mu\nu} R = \frac{8\pi G}{c^2} T_{\mu\nu} - \Lambda g_{\mu\nu}.$$

Possible interpretations:

- Λ: integration constant (cosmological constant), most general (covariant) expansion of Einstein's original equation
  Problem: Why is Λ so small, dominant today? Required fine-tuning in early universe. No explained from particle physics.
- $\Lambda g_{\mu\nu}$ as part of matter-energy tensor $T_{\mu\nu}$. Simplest case isotropic "fluid", $T_{\mu\nu} = \mathrm{diag}(\rho c^2, p, p, p)$. With $g_{\mu\nu} = \eta_{\mu\nu} = \mathrm{diag}(1, -1, -1, -1)$
  $\rightarrow p = -\rho c^2$, vacuum energy.
  Problem: Naive prediction wrong by 10^{120}!

Nature of dark energy?

Einstein equations:

$$R_{\mu\nu} - \frac{1}{2} g_{\mu\nu} R = \frac{8\pi G}{c^2} T_{\mu\nu} - \Lambda g_{\mu\nu}.$$

Possible interpretations:

- Dynamical dark energy (quintessence, K-essence, ...). Add time-dependence; add parameter w for equation of state: $p = w\rho c^2$. Holy grail of cosmology: Find $w \neq -1$, or $w(z)$!
  Problem: Still need fine-tuning.
- Move $\Lambda g_{\mu\nu}$ to left-hand side. Modification of Einstein's equation, modified gravity.
  Problem: Models not well constrained, some require fine-tuning. GR satisfied on very small and very large scales.

Gravitational lensing

Gravitational lensing = light deflection and focusing by matter

Light is deflected by both dark and luminous matter.

Important to study dark matter:

- Dominant over luminous (baryonic) matter (27% vs. 5%)
- Dark matter easy to understand and simulate (N-body simulations), only interaction is gravity

We will be looking at the small distortion of distant galaxies by the cosmic web (weak cosmological lensing, cosmic shear).

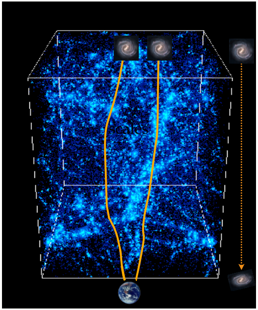

Brief history of gravitational lensing

- Before Einstein: Masses deflect photons, treated as point masses.
- 1915 Einstein's GR predicted deflection of stars by sun, deflection larger by 2 compared to classical value. Confirmed 1919 by Eddington and others during solar eclipse.

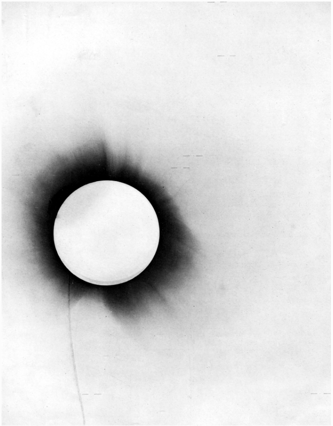

Photograph taken by Eddington of solar corona, and stars marked with bars.

Lensing on cosmological scales

- 1979 Walsh et al. detect first double image of a lenses quasar.

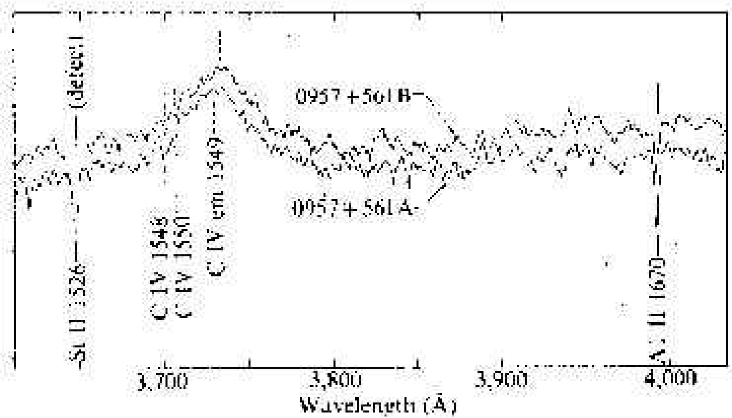

(Walsh et al. 1979)

- 1987 Soucail et al. strongly distorted "arcs" of background galaxies behind galaxy cluster, using CCDs.

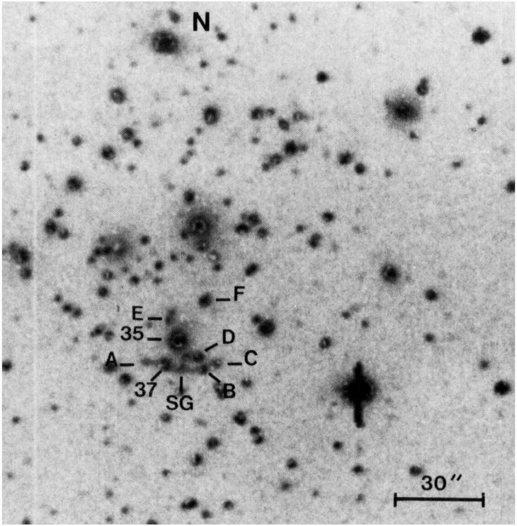

exclude that it is an off-chance superimposition of faint cluster galaxies even if a diffuse component seems quite clear from the R CCD field. A gravitational lens effect on a background quasar is a possibility owing to the curvature of the structure but in fact it is too small (Hammer 86) and no blue object opposite the central galaxy has been detected. It is more likely that we are dealing with a star formation region located in the very rich core where

- Tyson et al. (1990), tangential alignment around clusters.

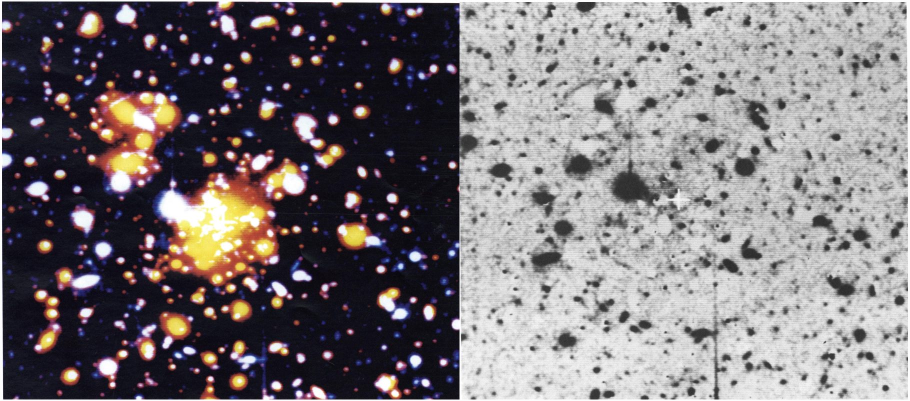

Abell 1689

Cluster outskirts: Weak gravitational lensing.

- 2000 cosmic shear: weak lensing in blind fields, by 4 groups (Edinburgh, Hawai'i, Paris, Bell Labs/US).
  Some $10,000$ galaxies on an area of a few square degrees on the sky.
- By 2018: Many dedicated surveys: DLS, CFHTLenS, DES, KiDS, HSC.
  Competitive constraints on cosmology.
  Factor 100 increase: Millions of galaxies over 100s of degrees. Many other improvements: Multi-band observations, photometric redshifts, image and N-body simulations, ...
- By 2025: LSST, WFIRST-AFTA, Euclid data will be available.
  Another factor of 100 increase: Hundred millions of galaxies, tens of thousands of degrees area (most of the extragalactic sky).

Light deflection

Simplest case: point mass deflects light

Deflection angle for a point mass M is

$$\hat{\alpha} = \frac{4GM}{c^2 \xi} = \frac{2R_{\rm S}}{\xi}$$

$R_{\rm S}$ is the Schwarzschild radius.
(Einstein 1915)

This is twice the value one would get in a classical, Newtonian calculation.

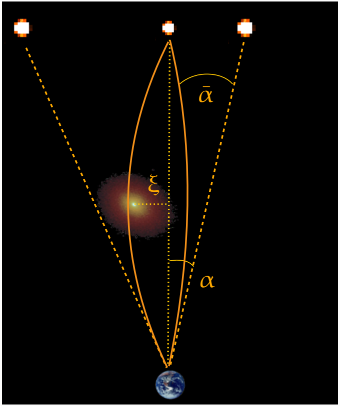

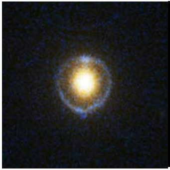

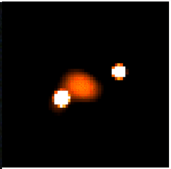

Deflection angle: general case

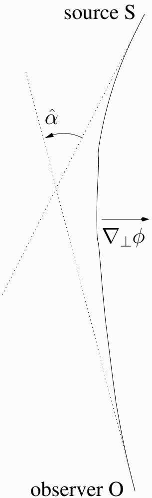

Perturbed Minkowski metric, weak-field ($\phi \ll c^2$)

$$\mathrm{d}s^2 = \left(1 + 2\phi/c^2\right) c^2 \mathrm{d}t^2 - \left(1 - 2\phi/c^2\right) \mathrm{d}\ell^2$$

One way to derive deflection angle: Fermat's principle of least light travel time.

Light travels on geodesics, $\mathrm{d}s^2 = 0$
$\rightarrow$ light travel time t is

$$t = \frac{1}{c} \int_{\text{path}} \left(1 - 2\phi/c^2\right) \mathrm{d}\ell$$

Deflection angle: general case

Fermat's principle: Minimize light travel time.
Analogous to refraction in medium with refractive index $n > 1$,

$$t = \frac{1}{c} \int_{\mathrm{path}} \left(1 - 2\phi/c^2\right) \mathrm{d}\ell = \frac{1}{c} \int_{\mathrm{path}} n(\boldsymbol{x}) \mathrm{d}\ell$$

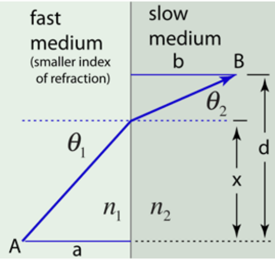

Minimize t to derive Snell's law, $\sin\theta_1 / \sin\theta_2 = n_2/n_1$.

Assume t is stationary, $\delta t = 0$.
Integrate Euler-Lagrange equations along the light path to get

$$\text{deflection angle} \qquad \hat{\boldsymbol{\alpha}} = -\frac{2}{c^2} \int_{\mathrm{S}}^{\mathrm{O}} \boldsymbol{\nabla}_\perp \phi \, \mathrm{d}\ell$$

Exercise: Derive the deflection angle for a point mass. I

Derive $\hat{\alpha} = 4GM/(c^2\xi)$.

We can approximate the potential as

$$\phi = -\frac{GM}{R} = -\frac{c^2}{2}\frac{R_\mathrm{S}}{R},$$

where G is Newton's constant, M the mass of the object, R the distance, and R_S the Schwarzschild radius
The distance R can be written as

$$R^2 = x^2 + y^2 + z^2.$$

(Weak-field condition $\phi \ll c^2$ implies $R \gg R_\mathrm{S}$.)
(Here z is not redshift, but radial (comoving) distance.)

We use the so-called Born approximation (from quantum mechanic scattering theory) to integrate along the unperturbed light ray, which is a straight line parallel to the z-axis with a constant $x^2 + y^2 = \xi^2$. The impact parameter ξ is the distance of the light ray to the point mass.

Exercise: Derive the deflection angle for a point mass. II

The deflection angle is then

$$\hat{\boldsymbol{\alpha}} = -\frac{2}{c^2} \int_{-\infty}^{\infty} \boldsymbol{\nabla}_\perp \phi \, \mathrm{d}z.$$

The perpendicular gradient of the potential is

$$\boldsymbol{\nabla}_\perp \phi = \frac{c^2 R_\mathrm{S}}{2|R|^3} \begin{pmatrix} x \\ y \end{pmatrix} = \frac{c^2 R_\mathrm{S}}{2} \frac{\xi}{(\xi^2 + z^2)^{3/2}} \begin{pmatrix} \cos\varphi \\ \sin\varphi \end{pmatrix}.$$

The primitive for $(\xi^2 + z^2)^{-3/2}$ is $z\xi^{-2}(\xi^2 + z^2)^{-1/2}]$. We use the symmetry of the integrand to integrate between 0 and ∞, and get for the absolute value of the deflection angle

$$\hat{\alpha} = 2R_\mathrm{S} \left[\frac{z}{\xi(\xi^2 + z^2)^{1/2}} \right]_0^\infty = \frac{2R_\mathrm{S}}{\xi} = \frac{4GM}{c^2 \xi}.$$

Generalisation I: mass distribution

Distribution of point masses $M_i(\boldsymbol{\xi}_i, z)$: total deflection angle is linear vectorial sum over individual deflections

$$\hat{\boldsymbol{\alpha}}(\boldsymbol{\xi}) = \sum_i \hat{\boldsymbol{\alpha}}(\boldsymbol{\xi} - \boldsymbol{\xi}_i) = \frac{4G}{c^2} \sum_i M_i(\boldsymbol{\xi}_i, z) \frac{\boldsymbol{\xi} - \boldsymbol{\xi}_i}{|\boldsymbol{\xi} - \boldsymbol{\xi}_i|}$$

Perform transition to continuous density, introduce 2D surface mass density Σ

$$M_i(\boldsymbol{\xi}_i, z) \to \int \mathrm{d}^2\xi' \int \mathrm{d}z' \, \rho(\boldsymbol{\xi}', z') = \int \mathrm{d}^2\xi' \, \Sigma(\boldsymbol{\xi}')$$

Can probe complex mass profiles ρ, or (2D projected) Σ.

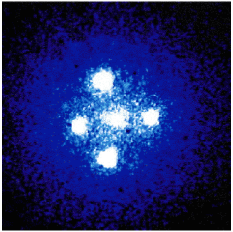

"Einstein cross", $z_\mathrm{s} = 1.7, z_\mathrm{l} = 0.04$

WFI2033-4723, $z_\mathrm{s} = 1.66, z_\mathrm{l} = 0.66$

Generalisation II: Extended source

Extended source: different light rays impact lens at different positions $\boldsymbol{\xi}$, their deflection angle $\boldsymbol{\alpha}(\boldsymbol{\xi})$ will be different: differential deflection $\rightarrow$ distortion, magnification of source image!

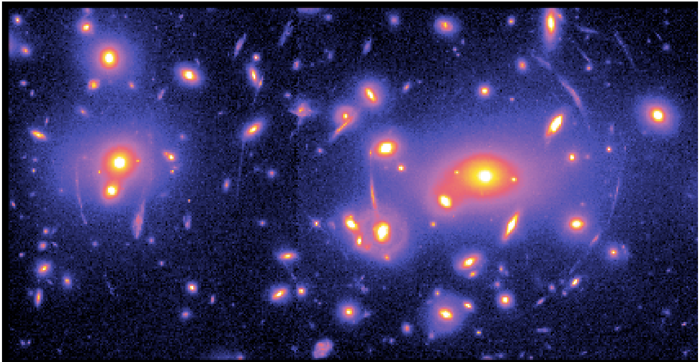

The cluster of galaxies Abell 2218

Lens equation

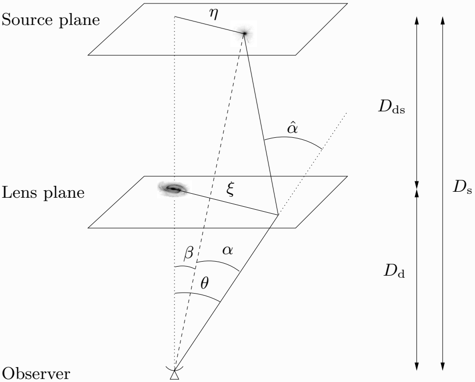

Defining rescaled deflection angle $\boldsymbol{\alpha} = \frac{D_{\rm ds}}{D_{\rm s}} \hat{\boldsymbol{\alpha}}$.
The simple equation relating lens to source extend is called lens equation

$$\boldsymbol{\beta} = \boldsymbol{\theta} - \boldsymbol{\alpha}(\theta).$$

This is a mapping from lens coordinates $\boldsymbol{\theta}$ to source coordinates $\boldsymbol{\beta}$. Why?

Cosmic shear: continuous deflection along line of sight

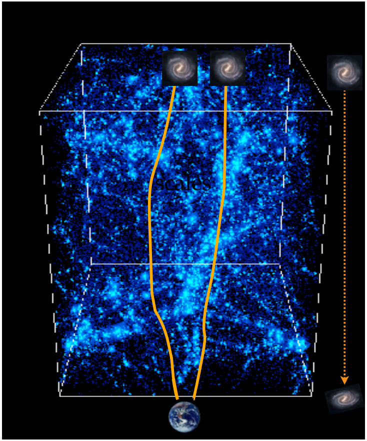

With the Born approximations, and assumption that structures along line of sight are un-correlated:

Deflection angle can be written as gradient of a potential, called lensing potential ψ:

$$\alpha(\boldsymbol{\theta}) = \boldsymbol{\nabla}\psi(\boldsymbol{\theta})$$

$$\psi(\boldsymbol{\theta}) = \frac{2}{c^2} \int_0^{\chi} \mathrm{d}\chi' \, \frac{\chi - \chi'}{\chi\chi'} \, \Phi(\chi'\boldsymbol{\theta}, \chi').$$

for a source at comoving distance χ.

Note: Difference between Born and actual light path up to few Mpc!

Linearizing the lens equation

We talked about differential deflection before. To first order, this involves the derivative of the deflection angle.

$$\frac{\partial \beta_i}{\partial \theta_j} \equiv A_{ij} = \delta_{ij} - \partial_j \alpha_i = \delta_{ij} - \partial_i \partial_j \psi.$$

Jacobi (symmetric) matrix

$$A = \begin{pmatrix} 1 - \kappa - \gamma_1 & -\gamma_2 \\ -\gamma_2 & 1 - \kappa + \gamma_1 \end{pmatrix}.$$

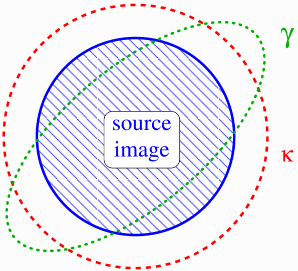

- convergence κ: isotropic magnification
- shear γ: anisotropic stretching

Convergence and shear are second derivatives of the 2D lensing potential.

Convergence and shear

The effect of κ and γ follows from Liouville's theorem: Surface brightness is conserved (no photon gets lost). We see that shear transforms a circular image into an elliptical one.

Define complex shear

$$\gamma = \gamma_1 + \mathrm{i}\gamma_2 = |\gamma| \mathrm{e}^{2\mathrm{i}\varphi};$$

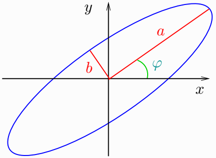

The relation between convergence, shear, and the axis ratio of elliptical isophotes is then

$$|\gamma| = |1-\kappa| \frac{1-b/a}{1+b/a}$$

Further consequence of lensing: magnification.
Liouville + area changes ($\mathrm{d}\beta^2 \neq \mathrm{d}\theta^2$ in general) $\rightarrow$ flux changes.

magnification $\quad \mu = \det A^{-1} = \left[(1-\kappa)^2 - \gamma^2\right]^{-1}.$

Convergence and cosmic density contrast

Back to the lensing potential

- Since $\kappa = \frac{1}{2}\Delta\psi$:

$$\kappa(\boldsymbol{\theta}, \chi) = \frac{1}{c^2} \int_0^\chi \mathrm{d}\chi' \, \frac{(\chi - \chi')\chi'}{\chi} \Delta_{\boldsymbol{\theta}} \Phi(\chi' \boldsymbol{\theta}, \chi')$$

- Terms $\Delta_{\chi'\chi'}\phi$ average out when integrating along line of sight, can be added to yield 3D Laplacian (error $\mathcal{O}(\phi) \sim 10^{-5}$).
- Poisson equation

$$\Delta\Phi = \frac{3H_0^2\Omega_\mathrm{m}}{2a}\,\delta \qquad \left(\delta = \frac{\rho - \bar\rho}{\rho}\right)$$

$$\rightarrow \kappa(\boldsymbol{\theta}, \chi) = \frac{3}{2}\Omega_\mathrm{m} \left(\frac{H_0}{c}\right)^2 \int_0^\chi \mathrm{d}\chi' \, \frac{(\chi - \chi')\chi'}{\chi a(\chi')} \, \delta\left(\chi' \boldsymbol{\theta}, \chi'\right).$$

Convergence with source redshift distribution

So far, we looked at the convergence for one single source redshift (distance χ). Now, we calculate κ for a realistic survey with a redshift distribution of source galaxies. We integrate over the pdf $p(\chi)\mathrm{d}\chi = p(z)\mathrm{d}z$, to get

$$\kappa(\boldsymbol{\theta}) = \int_0^{\chi_{\rm lim}} \mathrm{d}\chi \, p(\chi) \, \kappa(\boldsymbol{\theta}, \chi) = \int_0^{\chi_{\rm lim}} \mathrm{d}\chi \, G(\chi) \, \chi \, \delta\left(\chi\boldsymbol{\theta}, \chi\right)$$

with lens efficiency

$$G(\chi) = \frac{3}{2}\left(\frac{H_0}{c}\right)^2 \frac{\Omega_{\rm m}}{a(\chi)} \int_\chi^{\chi_{\rm lim}} \mathrm{d}\chi' \, p(\chi') \frac{\chi' - \chi}{\chi'}.$$

The convergence is a projection of the matter-density contrast, weighted by the source galaxy distribution and angular distances.

Parametrization of redshift distribution, e.g.

$$p(z) \propto \left(\frac{z}{z_0}\right)^{\alpha} \exp\left[-\left(\frac{z}{z_0}\right)^{\beta}\right]$$

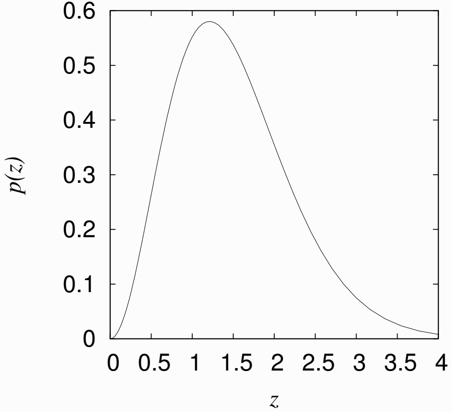

$\alpha = 2, \beta = 1.5, z_0 = 1$
(dashed line: all sources at redshift 1)

Max. lensing signal from halfway distance between us and lensing galaxies.

More on the relation between κ and γ

Convergence and shear are second derivatives of lensing potential $\rightarrow$ they are related.
One can derive κ from γ (except constant *mass sheet* κ_0).
E.g. get projected mass reconstruction of clusters from ellipticity observations.

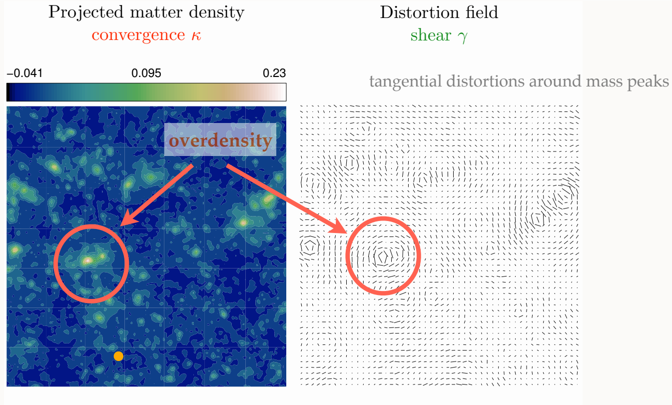

Source galaxies at $z = 1$, ray-tracing simulations by T. Hamana

Basic equation of weak lensing

Weak lensing regime

$\kappa \ll 1, |\gamma| \ll 1$.

The observed ellipticity of a galaxy is the sum of the intrinsic ellipticity and the shear:

$$\boxed{\varepsilon^{\mathrm{obs}} \approx \varepsilon^{\mathrm{s}} + \gamma}$$

Random intrinsic orientation of galaxies

$$\langle \varepsilon^{\mathrm{s}} \rangle = 0 \quad \longrightarrow \quad \boxed{\langle \varepsilon^{\mathrm{obs}} \rangle = \gamma}$$

The observed ellipticity is an unbiased estimator of the shear. Very noisy though! $\sigma_\varepsilon = \langle |\varepsilon^{\mathrm{s}}|^2 \rangle^{1/2} \approx 0.4 \gg \gamma \sim 0.03$. Increase S/N and beat down noise by averaging over large number of galaxies.

Question: Why is the equivalent estimation of the convergence and/or magnification more difficult?

Ellipticity and local shear

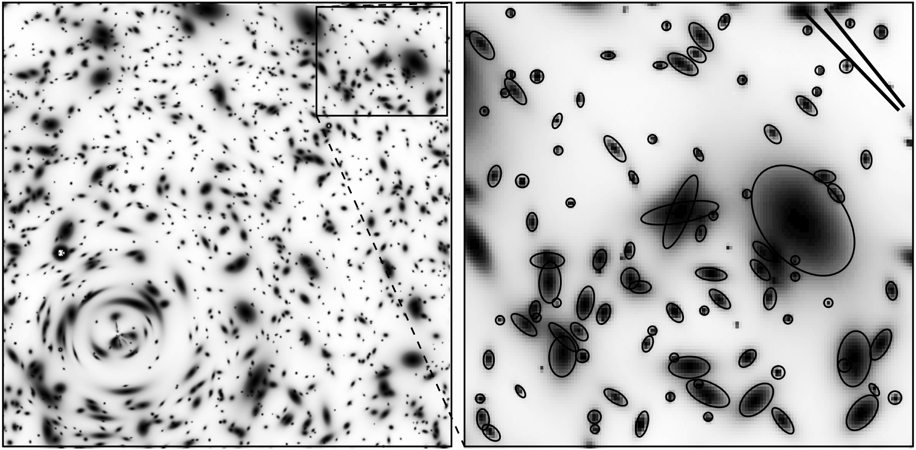

[from Y. Mellier]

Galaxy ellipticities are an estimator of the local shear.

More on the relation between κ and γ

Convergence and shear are second derivatives of lensing potential $\rightarrow$ they are related.
In particular, fluctuations (variance σ^2) in κ and γ are the same!

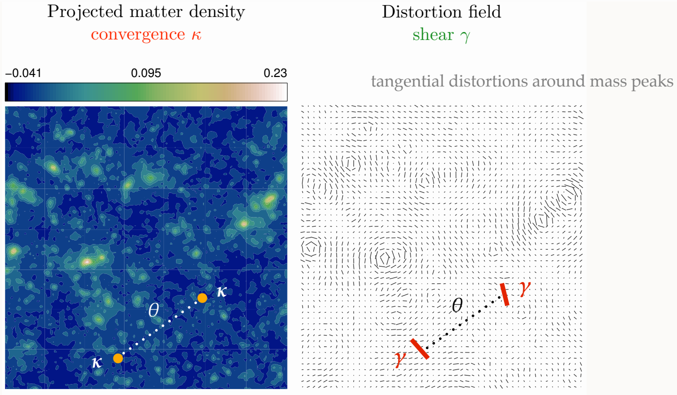

Source galaxies at $z = 1$, ray-tracing simulations by T. Hamana

Characterising density fluctuations

Goal:

Statistical description of the large-scale structure (cosmic web).
First define density contrast

$$\delta(\boldsymbol{x}, t) = \frac{\rho(\boldsymbol{x}, t) - \bar{\rho}(t)}{\bar{\rho}(t)}.$$

By definition the expectation value (or spatial mean) vanishes

$$\langle \delta \rangle = 0,$$

since $\langle \rho \rangle = \rho$, so no (statistical) information in first moment.
$\rightarrow$ go to second moment $\langle \delta^2 \rangle$
Including spatial information: two-point correlation funtion ξ

$$\langle \delta(\boldsymbol{x}) \delta(\boldsymbol{x} + \boldsymbol{r}) \rangle_{\boldsymbol{x}} =: \xi(\boldsymbol{r})$$

For statistical isotropic (rotational invariance) and homogeneous (translational invariance) random field δ:

$$\xi(\boldsymbol{r}) = \xi(r)$$

Characterising density fluctuations

Example: (galaxy) number density corrlelation function = excess probability of finding an object at distance r,

$$d^2p = \bar{n}^2 dV_1 dV_2 \left[1 + \xi(r)\right].$$

$\xi = 0$: Poisson distribution

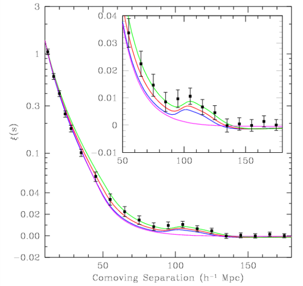

Measured galaxy correlation function, [SDSS].

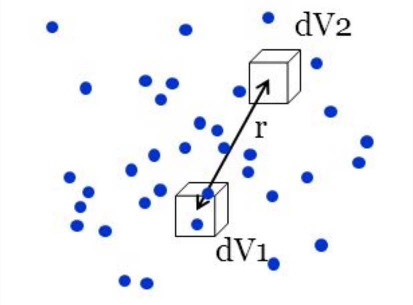

Characterising density fluctuations

Excess probability $\leftrightarrow$ more likely to find objects near other objects $\leftrightarrow$ clustering.

Clustering is a direct consequence of gravitational collapse in an expanding Universe.

Two-point correlation function only lowest-order statistic to describe field.

To quantify rich structure of voids, walls, filaments & clusters, need to go to higher-order correlations.

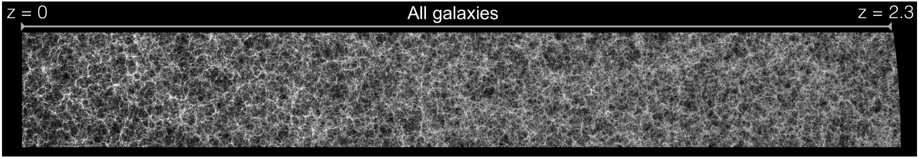

Euclid flagship simulations, (Potter et al. 2016)

The convergence power spectrum

- Variance of convergence $\langle \kappa(\boldsymbol{\vartheta} + \boldsymbol{\theta}) \kappa(\boldsymbol{\vartheta}) \rangle = \langle \kappa\kappa \rangle(\theta)$ depends on variance of the density contrast $\langle \delta\delta \rangle$.
- In Fourier space:

$$\left\langle \hat\kappa(\boldsymbol{\ell}) \hat\kappa^*(\boldsymbol{\ell}') \right\rangle = (2\pi)^2 \delta_{\rm D}(\boldsymbol{\ell} - \boldsymbol{\ell}') P_\kappa(\ell)$$

$$\left\langle \hat\delta(\boldsymbol{k}) \hat\delta^*(\boldsymbol{k}') \right\rangle = (2\pi)^3 \delta_{\rm D}(\boldsymbol{k} - \boldsymbol{k}') P_\delta(k)$$

- Limber's equation

$$P_\kappa(\ell) = \int \mathrm{d}\chi \, G^2(\chi) P_\delta \left(k = \frac{\ell}{\chi} \right)$$

  using small-angle approximation, $P_\delta(k) \approx P_\delta(k_\perp)$, contribution only from Fourier modes $\perp$ to line of sight. Also assumes that power spectrum varies slowly.

- It turns out that $\boxed{P_\kappa = P_\gamma}$

  So we use γ in observations, and κ in modelling.

Dependence on cosmology

initial conditions, growth of structure

$$P_\kappa(\ell) = \int \mathrm{d}\chi \, G^2(\chi) P_\delta\left(k = \frac{\ell}{\chi}\right)$$

$$G(\chi) = \frac{3}{2}\left(\frac{H_0}{c}\right)^2 \frac{\Omega_\mathrm{m}}{a(\chi)} \int_\chi^{\chi_\mathrm{lim}} \mathrm{d}\chi' \, p(\chi') \frac{\chi' - \chi}{\chi'}$$

matter density

redshift distribution of source galaxies

geometry

Lensing 'tomography' (2 1/2 D lensing)

- Bin galaxies in redshift.
- Lensing efficiency different for different bins: measure z-depending expansion and growth history.
- Necessary to measure dark energy, modified gravity.

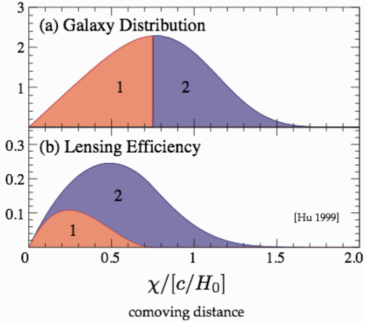

$$P_\kappa(\ell) = \int_0^{\chi_{\rm lim}} {\rm d}\chi\, G^2(\chi) P_\delta\left(k = \frac{\ell}{\chi}\right) \rightarrow$$

$$P_\kappa^{ij}(\ell) = \int_0^{\chi_{\rm lim}} {\rm d}\chi\, G_i(\chi) G_j(\chi) P_\delta\left(k = \frac{\ell}{\chi}\right)$$

$$G_i(\chi) = \frac{3}{2}\left(\frac{H_0}{c}\right)^2 \frac{\Omega_{\rm m}}{a(\chi)} \int_\chi^{\chi_{\rm lim}} {\rm d}\chi'\, p_i(\chi') \frac{\chi' - \chi}{\chi'}.$$

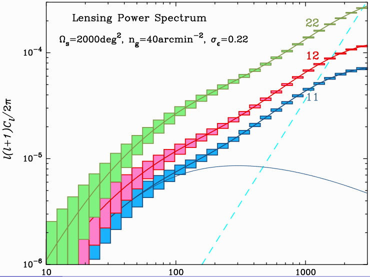

Lensing 'tomography' (2 1/2 D lensing)

- Bin galaxies in redshift.
- Lensing efficiency different for different bins: measure z-depending expansion and growth history.
- Necessary to measure dark energy, modified gravity.

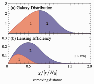

$$P_\kappa(\ell) = \int_0^{\chi_{\rm lim}} \mathrm{d}\chi\, G^2(\chi) P_\delta \left(k = \frac{\ell}{\chi}\right) \to$$

$$P_\kappa^{ij}(\ell) = \int_0^{\chi_{\rm lim}} \mathrm{d}\chi\, G_i(\chi) G_j(\chi) P_\delta \left(k = \frac{\ell}{\chi}\right)$$

$$G_i(\chi) = \frac{3}{2}\left(\frac{H_0}{c}\right)^2 \frac{\Omega_{\rm m}}{a(\chi)} \int_\chi^{\chi_{\rm lim}} \mathrm{d}\chi'\, p_i(\chi') \frac{\chi' - \chi}{\chi'}.$$

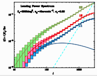

Question: Why does P_κ increase with z?

Comparison to CMB angular power spectrum

Unlike CMB C_ℓ's, features in matter power spectrum are washed out by projection and non-linear evolution.

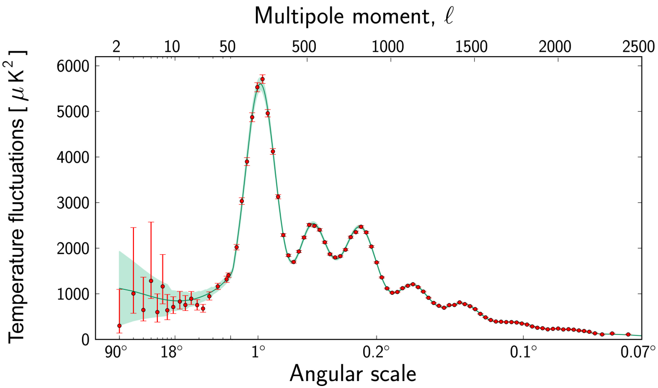

[Planck Consortium]

The shape measurement challenge

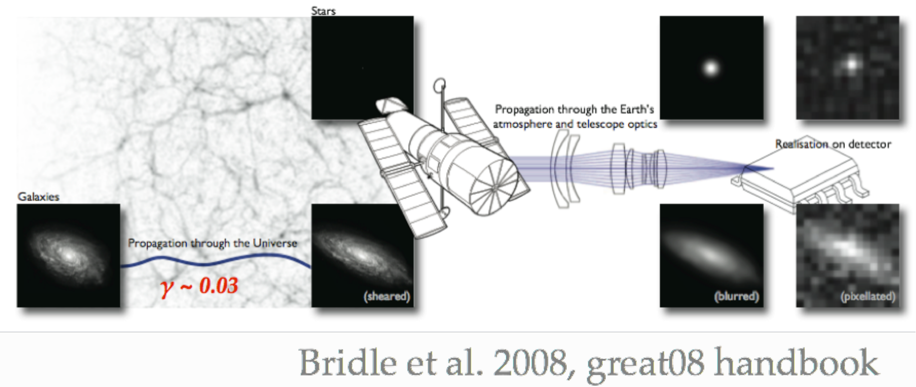

- Cosmological shear $\gamma \ll \varepsilon$ intrinsic ellipticity
- Galaxy images corrupted by PSF (point-spread function)
- Measured shapes are biased

Measuring cosmic shear

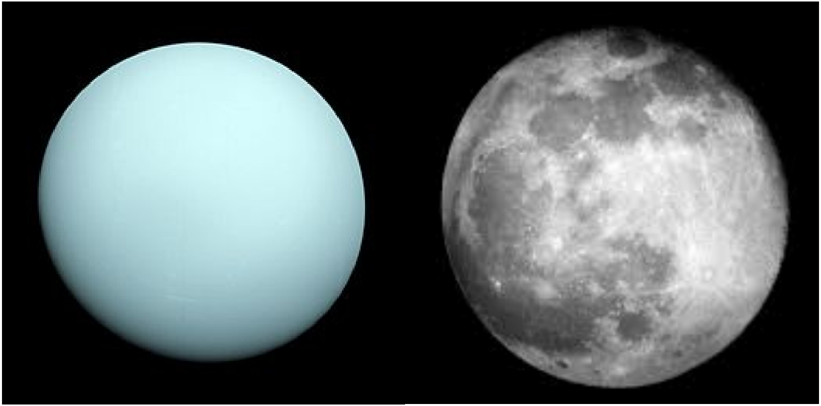

Typical shear of a few percent equivalent to difference in ellipticity between Uranus and the Moon.

The shape measurement challenge

How do we measure “ellipticity” for irregular, faint, noisy objects?

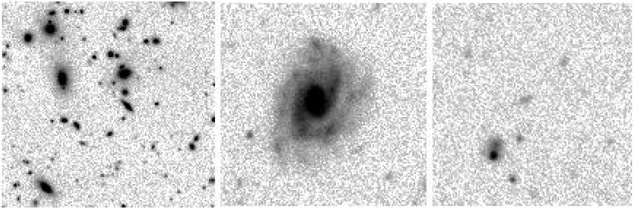

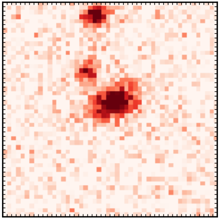

[Y. Mellier/CFHT(?)] — (Jarvis et al. 2016)

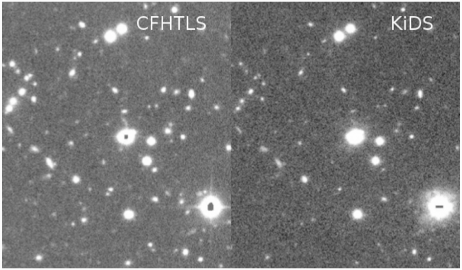

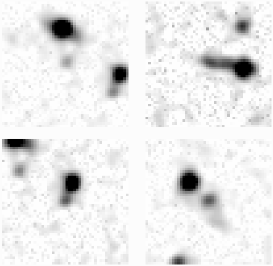

[CFHTLenS/KiDS image — CFHTlenS postage stamps]

Shape measurement

Example: Model fitting

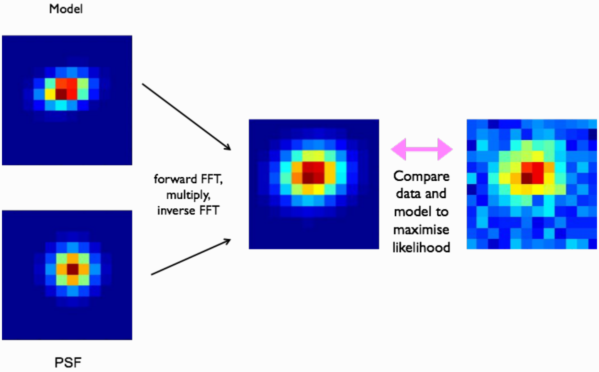

Forward model-fitting (example *lens*fit)

- Convolution of model with PSF instead of devonvolution of image
- Combine multiple exposures (in Bayesian way, multiply posterior density), avoiding co-adding of (dithered) images

Dithering


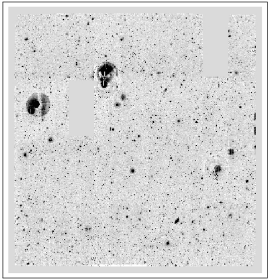
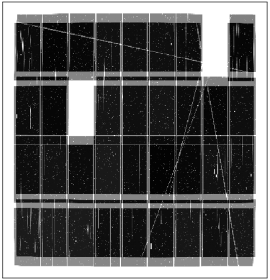

Left: Image of the MegaCam focal plane (CCDs arrays).

Middle: Co-add of two r-band exposures of CFHTLenS (without the 4 new CCDs).

Right: Weight map.

Shear measurement biases I

Origins

- **Noise bias**: In general, ellipticity is non-linear in pixel data (e.g. normalization by flux). Pixel noise $\rightarrow$ biased estimators.
- **Model bias**: Assumption about galaxy light distribution is in general wrong.
- **Other**: Imperfect PSF correction, detector effects (CTI — charge transfer inefficiency), selection effects (probab. of detection/sucessful ε measurement depends on ε and PSF)

Characterisation

Bias can be multiplicative ($\boldsymbol{m}$) and additive ($\boldsymbol{c}$):

$$\gamma_i^{\text{obs}} = (1+m)\gamma_i^{\text{true}} + c; \quad i = 1, 2.$$

Biases m, c are typically complicated functions of galaxy properties (e.g. size, magnitude, ellipticity), redshift, PSF, ... They can be scale-dependent.

Current methods: $|m| = 1\% - 10\%, |c| = 10^{-3} - 10^{-2}$.

Blind simulation challenges have been run to quantify biases, getting ideas from computer science community (e.g. `http://great3challenge.info`).

Shear measurement biases I

Origins

- **Noise bias**: In general, ellipticity is non-linear in pixel data (e.g. normalization by flux). Pixel noise → biased estimators.
- **Model bias**: Assumption about galaxy light distribution is in general wrong.
- **Other**: Imperfect PSF correction, detector effects (CTI — charge transfer inefficiency), selection effects (probab. of detection/sucessful ε measurement depends on ε and PSF)

Characterisation

Bias can be multiplicative ($\boldsymbol{m}$) and additive ($\boldsymbol{c}$):

$$\gamma_i^{\rm obs} = (1+m)\gamma_i^{\rm true} + c; \quad i = 1, 2.$$

Biases m, c are typically complicated functions of galaxy properties (e.g. size, magnitude, ellipticity), redshift, PSF, ... They can be scale-dependent.

Current methods: $|m| = 1\% - 10\%, |c| = 10^{-3} - 10^{-2}$.

Blind simulation challenges have been run to quantify biases, getting ideas from computer science community (e.g. `http://great3challenge.info`).

rgpp/rp = FWHM of PSF-convolved galaxy to PSF

Shear measurement biases II

Calibration

Functional dependence of m on observables must not be too complicated (e.g. not smooth, many variables, large parameter space), or else measurement is *not calibratable*!

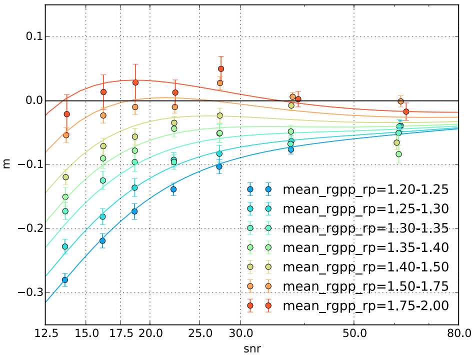

(Jarvis et al. 2016) - image simulations

Requirements for surveys

Necessary knowledge of residual biases $|\Delta m|, |\Delta c|$ (after calibration):
Current surveys 1%.
Future large missions (Euclid, LSST, ...) $10^{-4} = 0.1\%$!

PSF correction

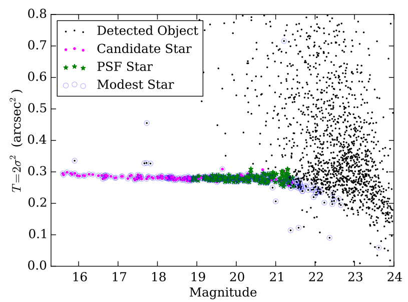

(Jarvis et al. 2016)

- Select clean sample of stars
- Measure star shapes
- Create PSF model and interpolate (pixel values, ellipticity, PCA coefficients, ...) to galaxy positions. Space-based observations: global PSF model from many exposures possible
- Correct for PSF: galaxy image devonvolution or other (e.g. linearized) correction, or convolve model

PSF correction

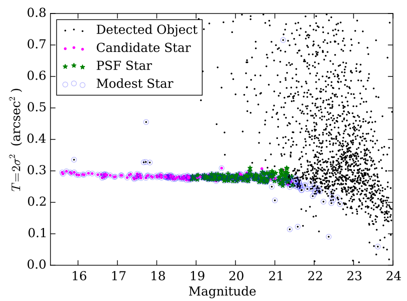

(Jarvis et al. 2016)

- Select clean sample of stars
- Measure star shapes
- Create PSF model and interpolate (pixel values, ellipticity, PCA coefficients, ...) to galaxy positions. Space-based observations: global PSF model from many exposures possible
- Correct for PSF: galaxy image devonvolution or other (e.g. linearized) correction, or convolve model

PSF correction

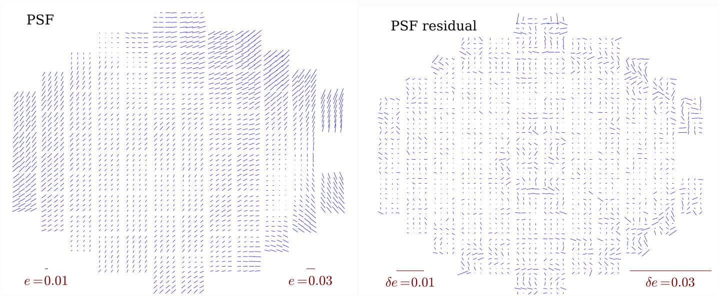

(Jarvis et al. 2016)

- Select clean sample of stars
- Measure star shapes
- Create PSF model and interpolate (pixel values, ellipticity, PCA coefficients, ...) to galaxy positions. Space-based observations: global PSF model from many exposures possible
- Correct for PSF: galaxy image devonvolution or other (e.g. linearized) correction, or convolve model

PSF correction

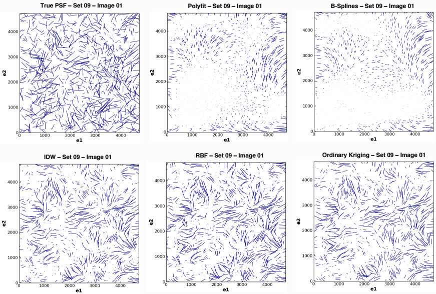

(Gentile et al. 2013)

- Select clean sample of stars
- Measure star shapes
- Create PSF model and interpolate (pixel values, ellipticity, PCA coefficients, ...) to galaxy positions. Space-based observations: global PSF model from many exposures possible
- Correct for PSF: galaxy image devonvolution or other (e.g. linearized) correction, or convolve model

PSF correction

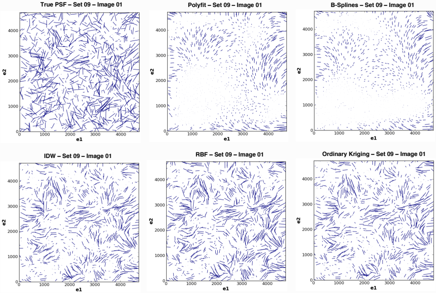

(Gentile et al. 2013)

- Select clean sample of stars
- Measure star shapes
- Create PSF model and interpolate (pixel values, ellipticity, PCA coefficients, ...) to galaxy positions. Space-based observations: global PSF model from many exposures possible
- Correct for PSF: galaxy image devonvolution or other (e.g. linearized) correction, or convolve model

PSF interpolation

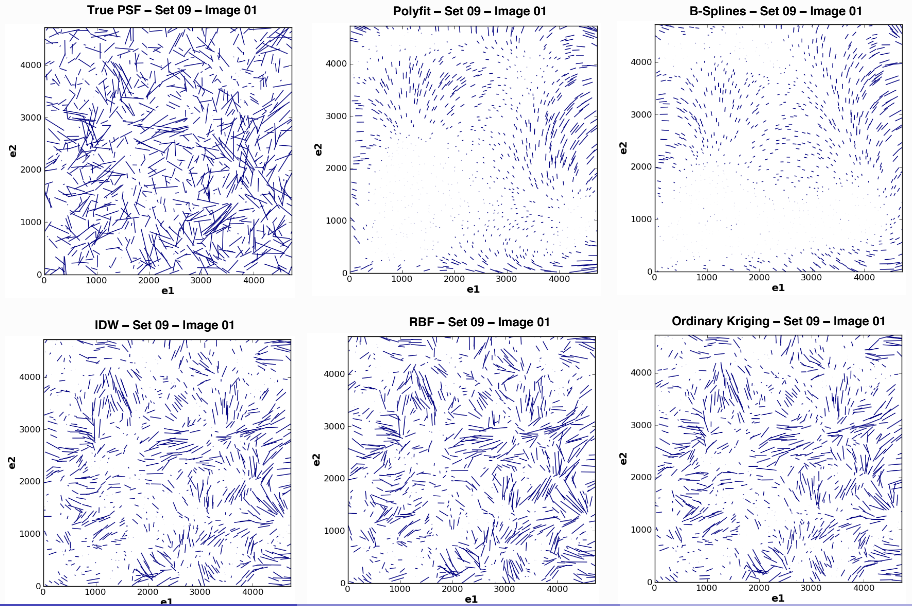

Results from weak-lensing surveys

1. Early era: 2000 - 2006
2. Consolidating era: 2007 – 2012
3. Small-survey era: 2013 – 2016
4. Medium survey era: 2017 – 2021
5. Large survey era: 2022 – 2030

State of the art ~ 2013: CFHTLenS

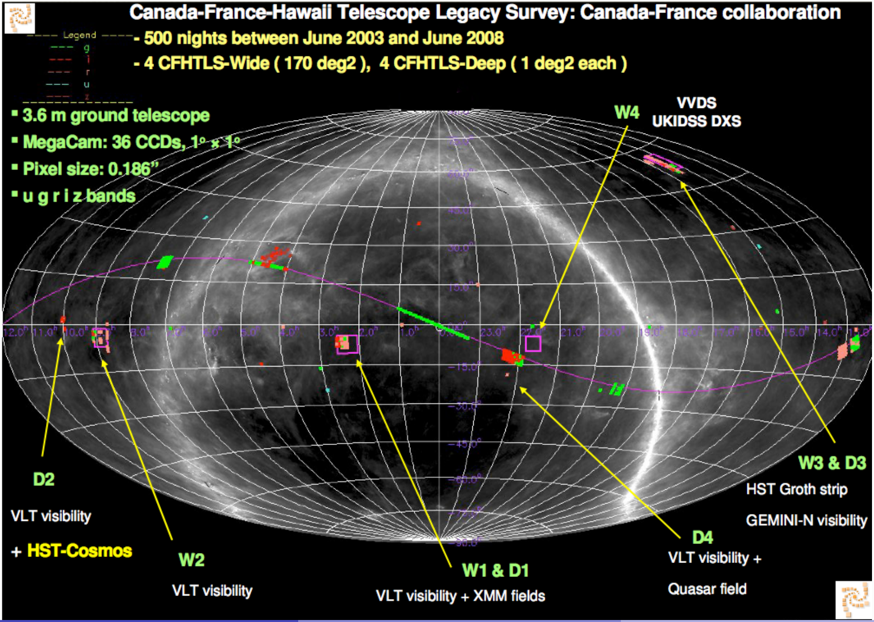

State of the art $\sim$ 2013

CFHTLenS

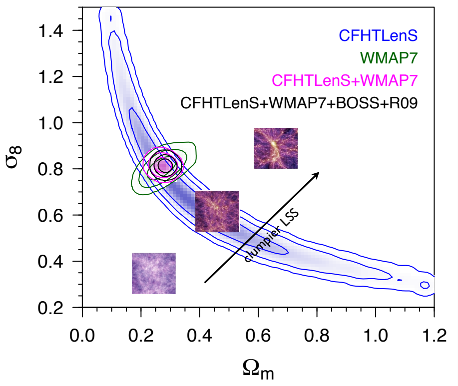

2D lensing
(Kilbinger et al. 2013)

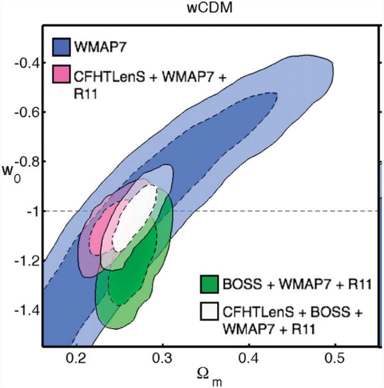

6-bin tomography
(Heymans et al. 2013)

(σ_8: power-spectrum normalisation; RMS of density fluct. in 8 Mpc spheres.)

Ongoing surveys: KiDS

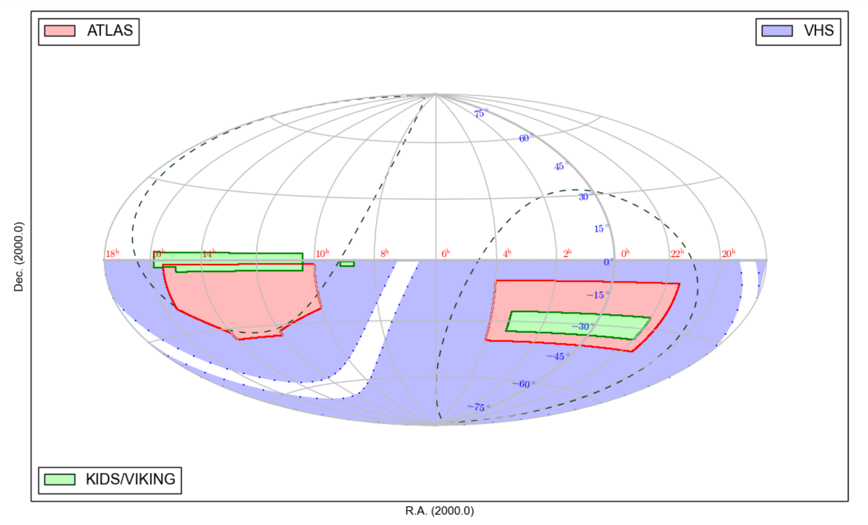

Ongoing surveys: DES

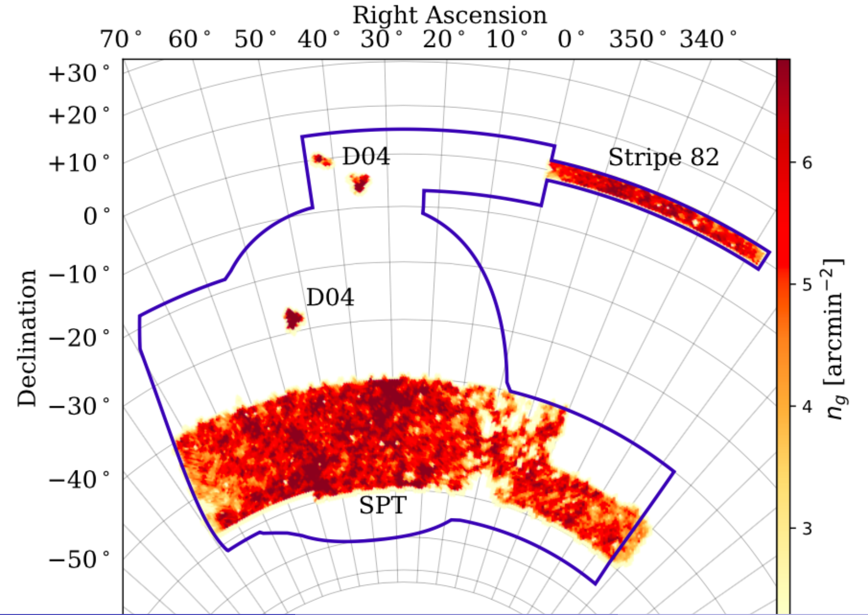

More recent results ∼ 2017

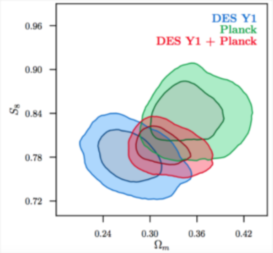

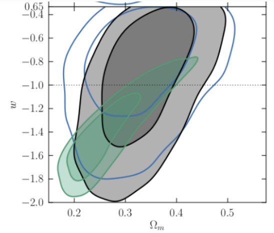

(DES Coll. et al. 2017) - DES WL + GC (Troxel et al. 2017) - DES

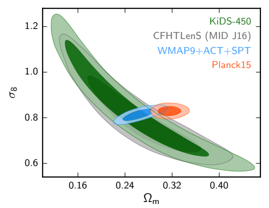

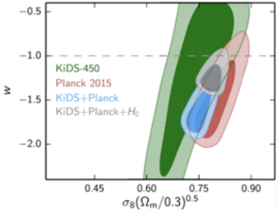

(Hildebrandt et al. 2017) - KiDS (Joudaki et al. 2017) - KiDS

ESA Euclid mission:

- \- Total mass satellite :
- 2 200 kg
- \- Dimensions:
- 4,5 m x 3 m
- \- Launch: end 2020 by a Soyuz rocket from the Kourou space port
- Euclid placed in L2
- \- Survey: 6 years,

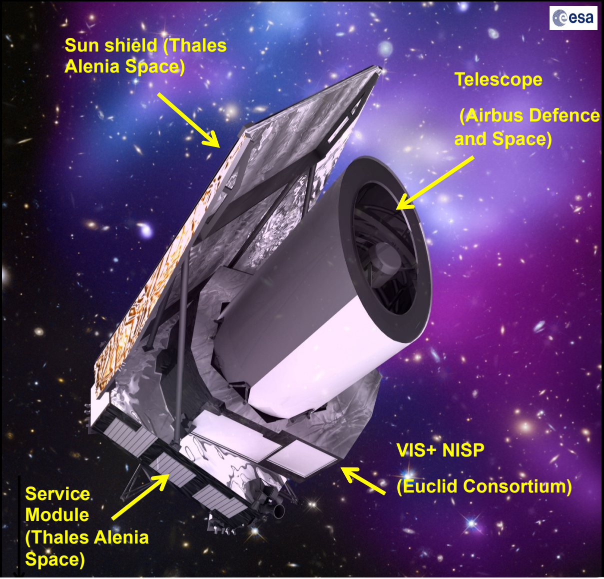

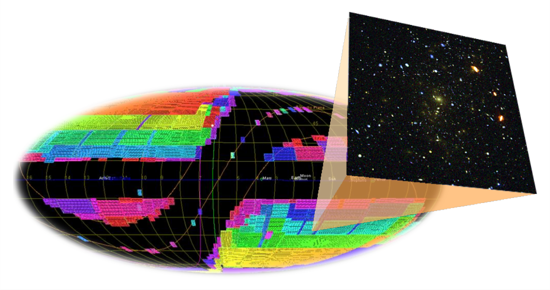

Euclid area = 15,000 deg^2 (extra-galaxtic and -ecliptic sky).

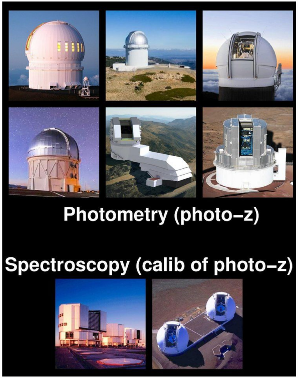

Ground-based observations for photometric redshifts.

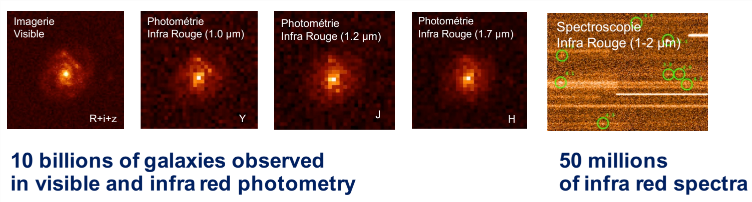

Euclid imaging and spectroscopy.

Euclid

Two instruments:

- Visible imager, WL, 1.5×10^9 galaxies
- Near-IR imager + spectrograph, 3×10^7 galaxy spectra

Cosmology

- Dark-energy equation of state w to 2% (currently $\sim 20\%$)
- Constrain models of modified gravity
- Neutrino masses to 0.02 eV (currently ~ 0.3 eV)
- Map dark matter distribution
- Early-universe conditions, inflation: limit non-Gaussianity $f_{\rm NL}$ to ± 2 (currently $\sim \pm 6$)

"Legacy"

- High-redshift galaxies, AGN & clusters @ $z > 1$, QSO @ $z > 8$, strong lensing galaxy candidates: Increase of numbers by several orders of magnitude

SLACS (~2010 - HST): gravitational lensing by galaxies

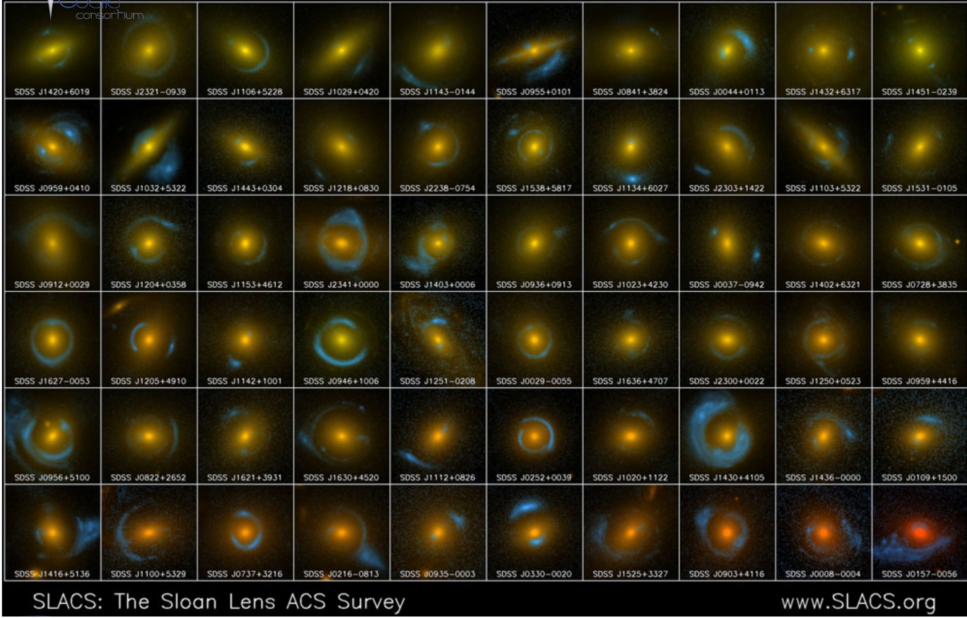


SLACS
Euclid VIS Legacy : after 2 months
(66 months planned)
140,000 strong lenses by galaxies, 5000 giant arcs in clusters

Euclid instruments

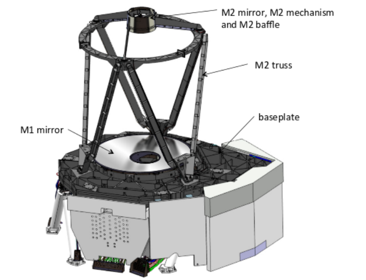

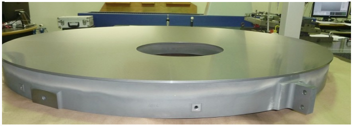

Structure and primary mirror

Near-Infrared instrument →

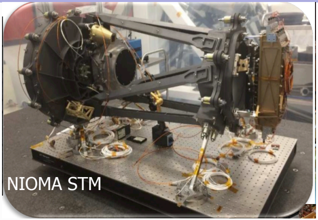

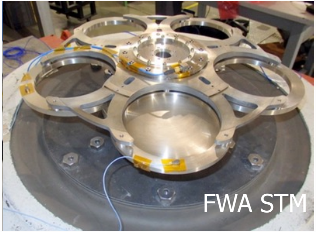

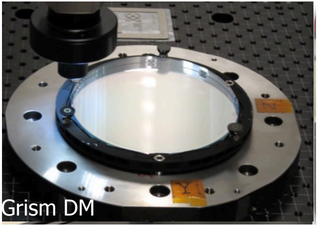

Visible imager instrument testing

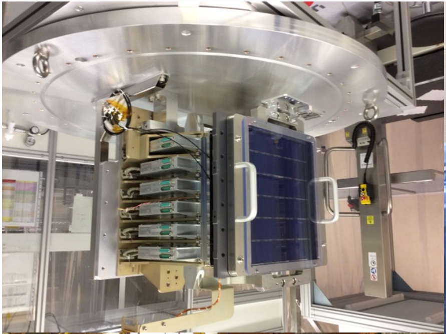

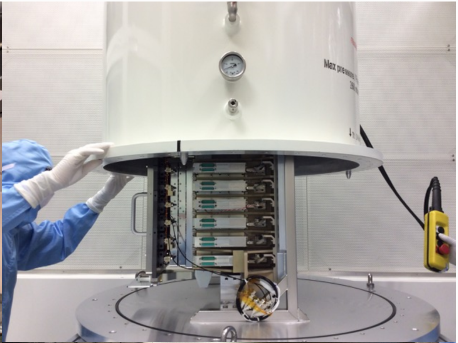

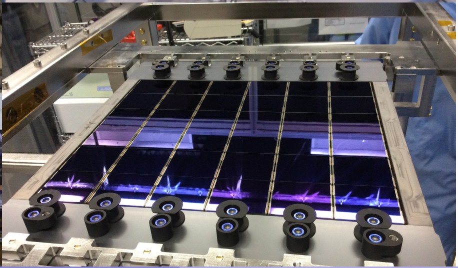

Weak-lensing mass maps @ very high resolution

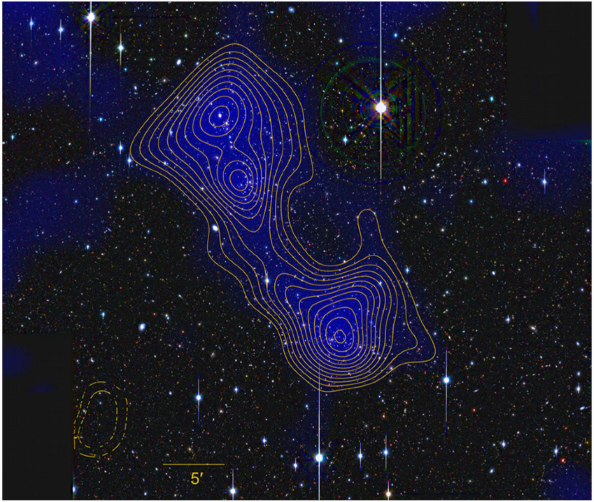

A 222/223, filament between clusters (Dietrich et al. 2012)

Euclid imaging

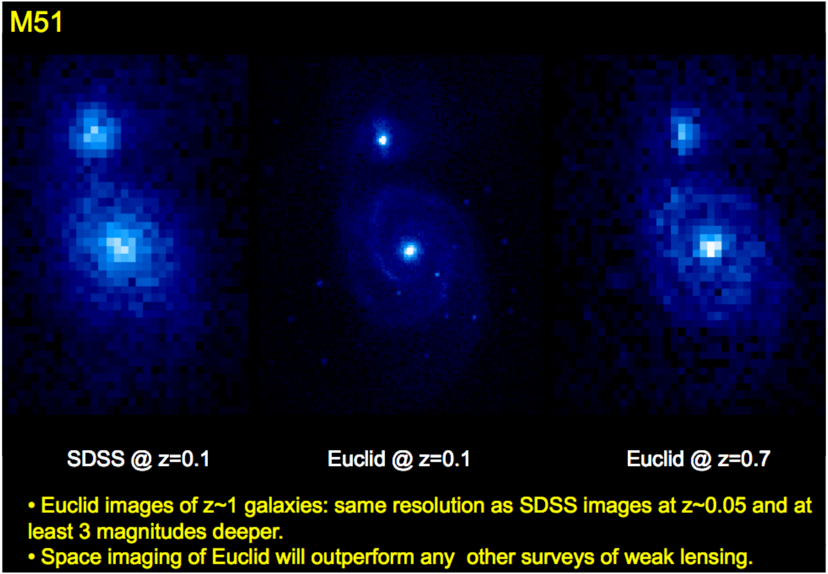

Euclid WL challenges

Under-sampled PSF

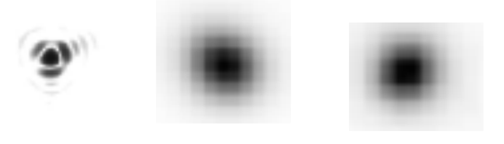

True and observed PSF (two realisations)

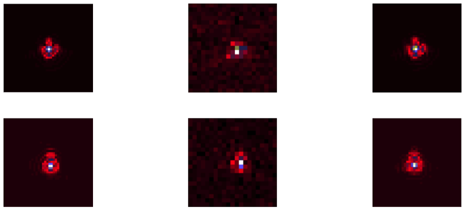

(a) True high-res PSF (b) Observed (c) Reconstruction

PSF super-resolution and denoising with sparsity-based RCA (Resolved Components Analysis), (Ngolè Mboula et al. 2016)

Euclid WL challenges

CTI: Charge-transfer inefficiency

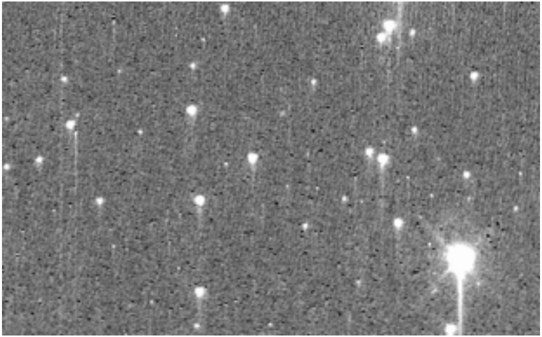

CTI stems from electron traps in CCD pixels. Trails depend on CCD read-out direction, distance from border, object brightness.
Non-convolutional effect. Can be modelled and corrected, but imperfectly due to noise.
Degrades with time (cosmic ray bombarding).

Euclid WL challenges

Cosmic rays, CTI (charge transfer inefficiency)
Corrected simulated Euclid image

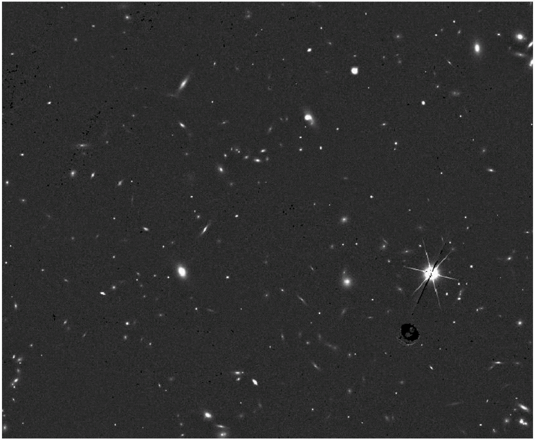

Simulations: Henry McCracken & VIS team (IAP).

Euclid WL challenges

Cosmic rays, CTI (charge transfer inefficiency)

Uncorrected simulated Euclid image

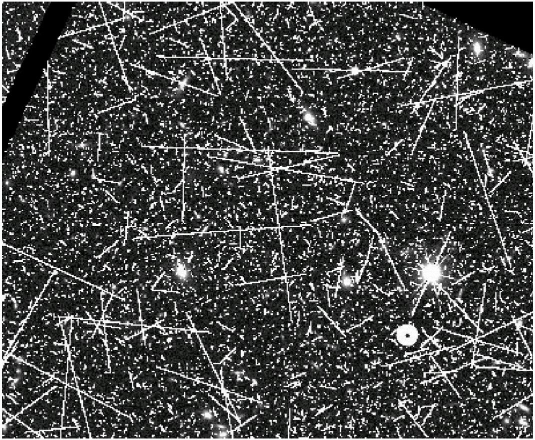

Simulations: Henry McCracken & VIS team (IAP).

Euclid VIS: CTI effects

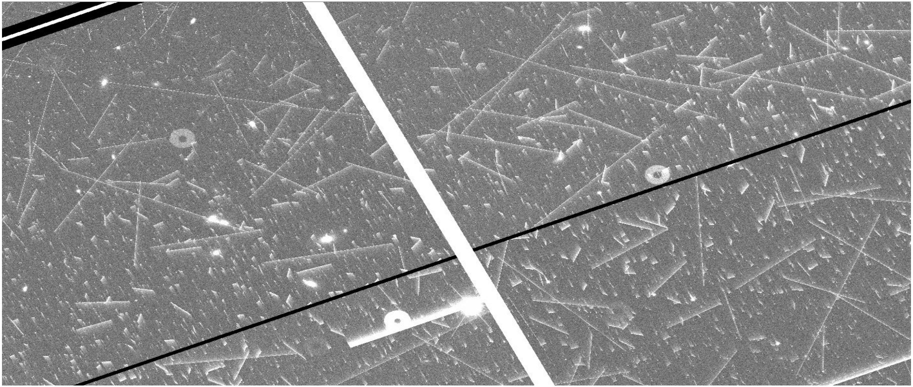

Euclid simulation zoom-in.

Euclid VIS: Mosaic

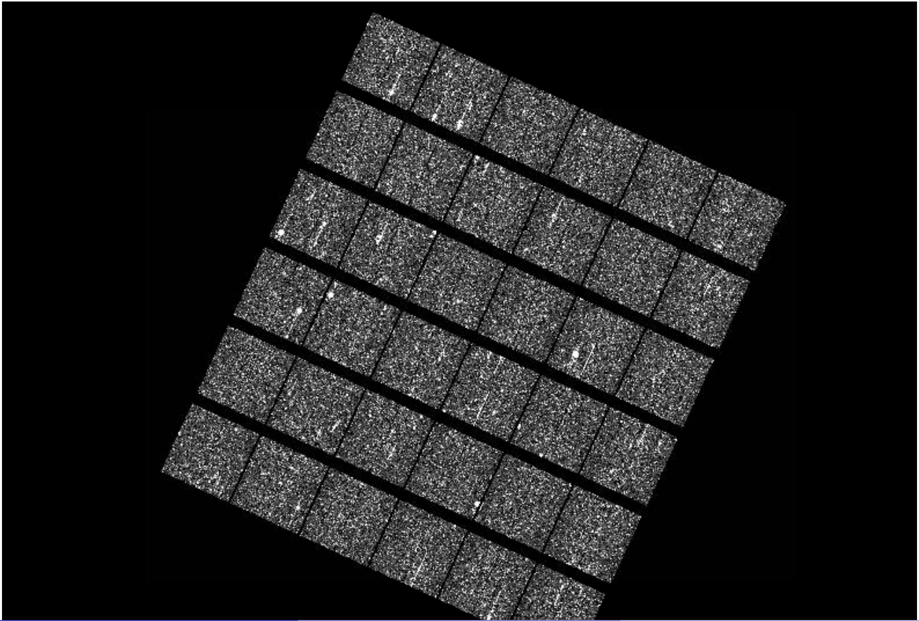

Euclid WL challenges

Color gradients

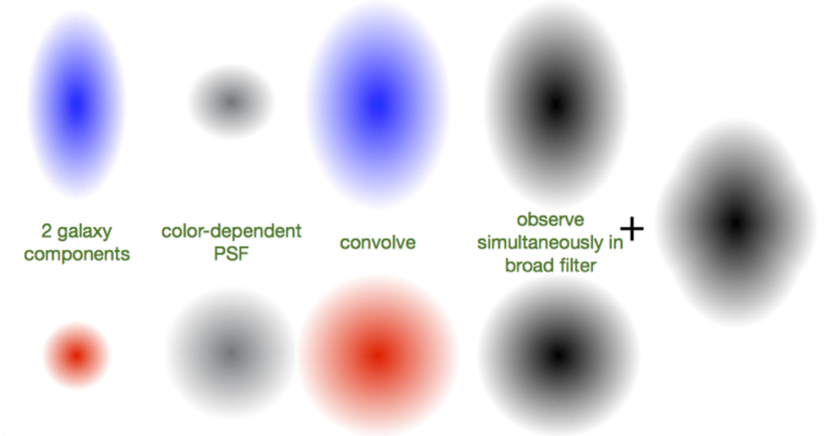

Euclid observes without optical filter (equiv. $R + I + z$). Calibrate color effects using HST multi-band observations.

Euclid WL challenges: Simulating the sky

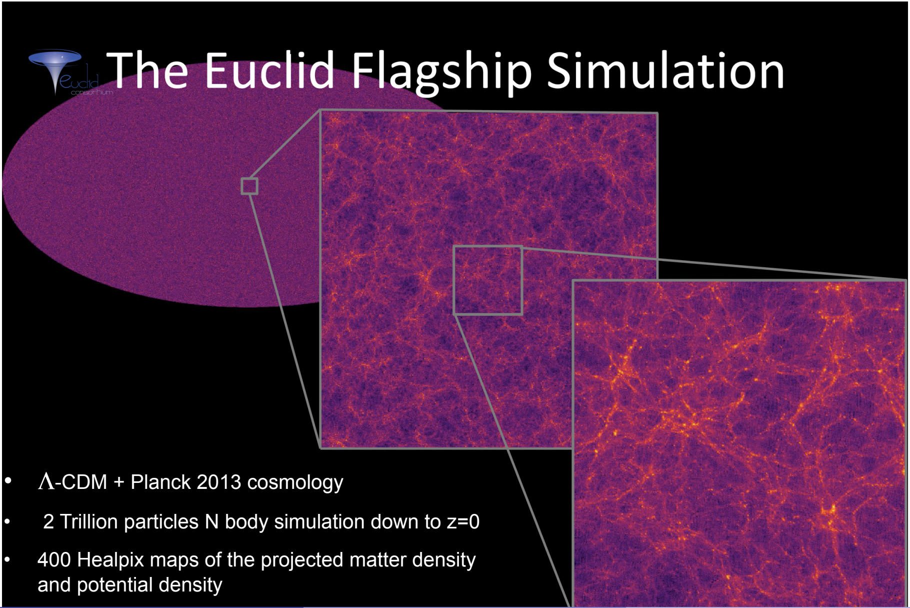

The bullet cluster and the nature of dark matter

The bullet cluster

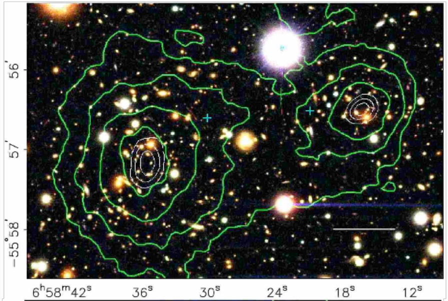

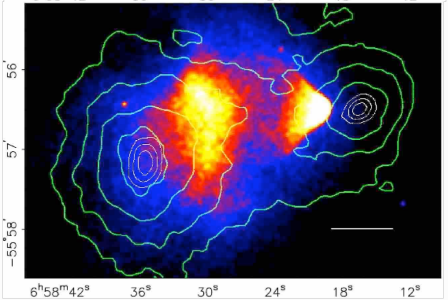

Clowe et al. (2006)

- Merging galaxy cluster at $z = 0.296$
- Recent major merger 100 Myr ago
- Components moving nearly perpendicular to line of sight with $v = 4700$ km s^{-1}
- Galaxy concentration offset from X-ray emission. Bow shocks visible

The bullet cluster: strong lensing

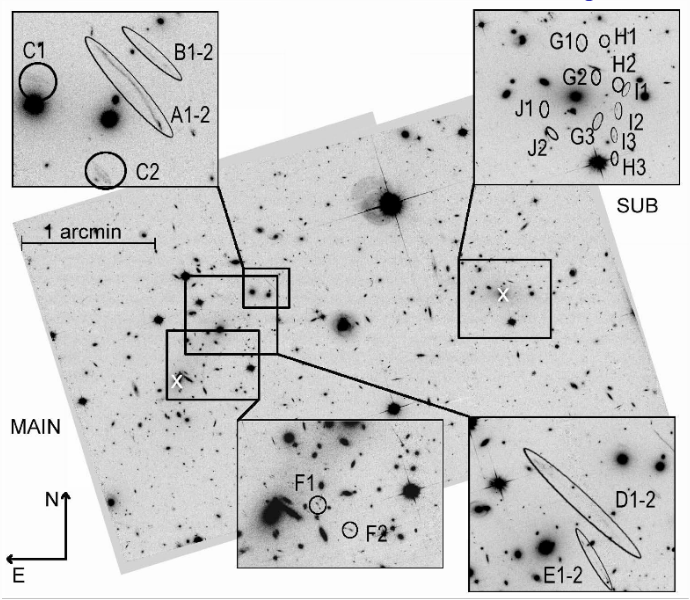

The bullet cluster: WL and X-ray

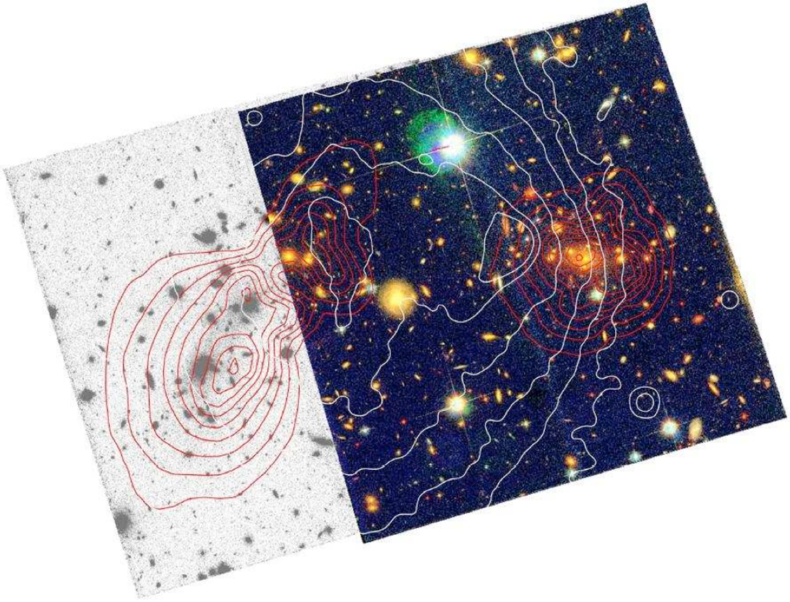

The bullet cluster: Evidence for dark matter

- $10\sigma (6\sigma)$ offset between main (sub-)mass peak and X-ray gas → most cluster mass is not in hot X-ray gas (unlike most baryonic mass: $m_X \gg m_*$!)
- Main mass associated with galaxies → this matter is collisionless

Modified gravity theories without dark matter: MoND (Modified Newtonian Dynamics), (Milgrom 1983), changes Newton's law for low accelerations ($a \sim 10^{-10}$ m s^{-2}), can produce flat galaxy rotation curves and Tully-Fisher relation.
MoND's relativistic version (Bekenstein 2004), varying gravitational constant $G(r)$. Introduces new vector field ("phion") with coupling strenght $\alpha(r)$ and range $\lambda(r)$ as free functions.
This can produce non-local weak-lensing convergence mass, where $\kappa \not\propto \delta$!
Necessary to explain offset between main κ peak and main baryonic mass.
Model with four mass peaks can roughly reproduce WL map with additional collisionless mass! E.g. 2 eV neutrinos.

The bullet cluster: MoND model

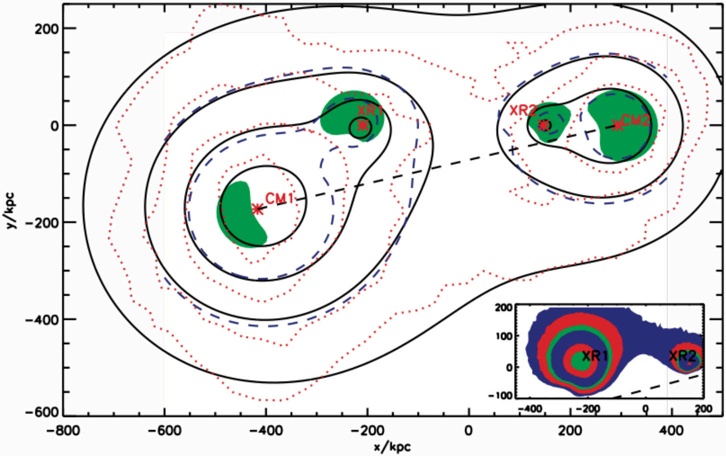

FIG. 1.— Our fitted convergence map (solid black lines) overplotted on the convergence map of C06 (dotted red lines) with x and y axes in kpc. The contours are from the outside 0.16,0.23,0.3 and 0.37. The centres of the four potentials we used are the red stars which are labelled. Also overplotted (blue dashed line) are two contours of surface density [4.8 & 7.2]$\times 10^2 M_\odot$ pc^{-2} for the MOND standard μ function; note slight distortions compared to the contours of κ. The green shaded region is where matter density is above $1.8\times10^{-3} M_\odot$ pc^{-3} and correspond to the clustering of 2eV neutrinos. *Inset:* The surface density of the gas in the bullet cluster predicted by our collisionless matter subtraction method for the standard μ-function. The contour levels are [30, 50, 80, 100, 200, 300]$M_\odot pc^{-2}$. The origin in RA and dec is [$06^h 58^m 24.38^s$,-55^{o}56'.32]

Bibliography I

Bekenstein J D 2004 *Phys. Rev. D* **70**(8), 083509.

DES Coll., Abbott T M C, Abdalla F B, Alarcon A, Aleksić J & al. 2017 *arXiv* **1708.01530**.

Einstein A 1915 *Sitzungsberichte der Königlich Preußischen Akademie der Wissenschaften (Berlin), Seite 844-847.* .

Gentile M, Courbin F & Meylan G 2013 *A&A* **549**, A1.

Heymans C, Grocutt E, Heavens A, Kilbinger M, Kitching T D & al. 2013 *MNRAS* **432**, 2433–2453.

Hildebrandt H, Viola M, Heymans C, Joudaki S, Kuijken K & al. 2017 *MNRAS* **465**, 1454–1498.

Jarvis M, Sheldon E, Zuntz J, Kacprzak T, Bridle S L & al. 2016 *MNRAS* **460**, 2245–2281.

Joudaki S, Mead A, Blake C, Choi A, de Jong J & al. 2017 *MNRAS* **471**, 1259–1279.

Kilbinger M, Fu L, Heymans C, Simpson F, Benjamin J & al. 2013 *MNRAS* **430**, 2200–2220.

Mandelbaum R 2017 *submitted to ARA&A, arXiv* **1710.03235**.

Bibliography II

Milgrom M 1983 *Astrophysical Journal* **270**, 371–389.

Ngolè Mboula F M, Starck J L, Okumura K, Amiaux J & Hudelot P 2016 *ArXiv e-prints* .

Potter D, Stadel J & Teyssier R 2016 *ArXiv e-prints* .

Springel V, White S D M, Jenkins A, Frenk C S, Yoshida N & al. 2005 *Nature* **435**, 629–636.

Troxel M A, MacCrann N, Zuntz J, Eifler T F, Krause E & al. 2017 *arXiv* **1708.01538**.

Walsh D, Carswell R F & Weymann R J 1979 *Nature* **279**, 381–384.